THE JOURNAL OF PHYSICAL CHEMISTRY A
A JOURNAL OF THE AMERICAN CHEMICAL SOCIETY

pubs.acs.org/JPCA Article

Mg−Fe Bonding in the $MgFe(CO)_n^+$ (n = 4−9) Cation Complexes: An Infrared Photodissociation Spectroscopic and Theoretical Study

Xiaoyang Jin, Yangyu Zhou, Guanjun Wang, and Mingfei Zhou*

Cite This: J. Phys. Chem. A 2023, 127, 4483−4491 Read Online

ABSTRACT: Heteronuclear magnesium−iron carbonyl cation complexes $MgFe(CO)_n^+$ (n = 4−9) are prepared in the gas phase and are detected by mass-selected infrared photodissociation spectroscopy in the carbonyl stretching frequency region. The geometric structures and the metal−metal bonding are discussed with the aid of quantum chemical calculations. The $MgFe(CO)_9^+$ cation is a coordinatively saturated complex. Each complex is characterized to contain more than one isomer. The small complexes (n = 4−6) possess the Mg−Fe bonded $[(OC)_{n-4}Mg-Fe(CO)_4]^+$ and/or $[(OC)_{n-5}Mg-Fe(CO)_5]^+$ structures with all the carbonyl ligands terminally bonded. For the larger complexes with n = 7−9, the $[(OC)_{n-4}Mg-Fe(CO)_4]^+$ structure is the major isomer experimentally observed. In addition, the $[(OC)_{n-5}Mg-OC-Fe(CO)_4]^+$ isomer involving a linear bridging carbonyl ligand is also characterized. Bonding analyses indicate that each $[(OC)_{n-4}Mg-Fe(CO)_4]^+$ complex contains a Mg−Fe electron-sharing σ bond. The metal−metal bond is described as a Mg(+I)−Fe(0) bond in $MgFe(CO)_4^+$ and as a Mg(+II)−Fe(−I) bond in the larger n = 5−9 complexes.

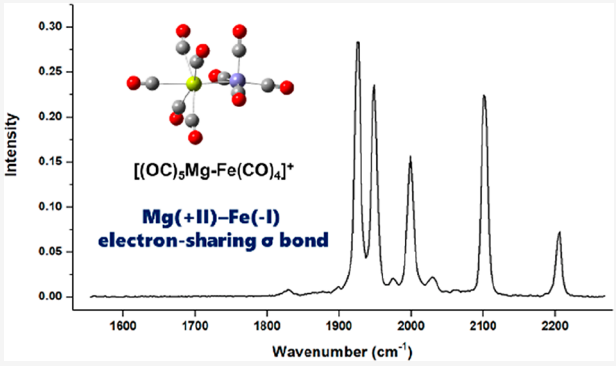

■ INTRODUCTION

Metal−metal bonded complexes have been intensively studied for decades, not only due to their various applications in catalysis, molecule activation and enzyme mimicry but also for fundamental understanding of metal−metal bonding.[1−6] Although this area was once dominated by d- and f-block metals,[7−10] considerable progress has also been achieved for metal−metal bonding containing p-block main group metals.[11−15] As electropositive s-block metals, alkaline earth metals are well-known in forming ionic or coordination compounds in the fully oxidized +2 oxidation state, whose covalent bonding properties were not taken seriously until recent years.[11−28] A milestone on alkaline earth metal−metal bonding was reached in 2007, when the first stable Mg(I)−Mg(I) bonded complex LMg−MgL (L = bulky guanidinate or β-diketiminate) was reported by Jones and co-workers.[29] Since then, a class of complexes containing the homonuclear Mg(I)−Mg(I) bond have been synthesized, which are considered as widely applicable, quasi-universal reducing agents in organic and inorganic synthesis.[30−34] Very recently, a trinuclear (BDI)MgMgMg(BDI) complex was reported, which is confirmed to contain a mixed-valence Mg(I)−Mg(0)−Mg(I) bonding unit.[35]

Magnesium can also form heteronuclear metal−metal bonds with either d-block or p-block metals. Since the first unsupported Mg−Fe bonded complex synthesized in 1974,[36] quite a few examples of heteronuclear complexes involving Mg−Fe, Mg−Co, Mg−Mn, Mg−Zn, and Mg−Al bonds have been reported.[37−44] Recently, the heteronuclear anion complexes $MgFe(CO)_4^-$ and $Mg_2Fe(CO)_4^-$ were generated in the gas phase and were studied by infrared photodissociation spectroscopy in this laboratory. Both complexes are characterized to contain an electron-sharing Mg(I)−Fe(−II) σ bond. The $Mg_2Fe(CO)_4^-$ complex involves a relatively weak covalent Mg(0)−Mg(I) σ bond.[45] Here we report the gas-phase generation and spectroscopic characterization of heteronuclear magnesium−iron carbonyl cation complexes $MgFe(CO)_n^+$ (n = 4−9). Infrared photodissociation spectroscopy combined with theoretical calculations confirm that the $MgFe(CO)_9^+$ is a coordinatively saturated complex and each complex possesses a $[(OC)_{n-4}Mg-Fe(CO)_4]^+$ structure containing an electron-sharing Mg−Fe σ bond.

■ EXPERIMENTAL AND COMPUTATIONAL METHODS

The heteronuclear magnesium−iron carbonyl cation complexes were produced in the gas phase by a pulsed laser vaporization/supersonic expansion source, and were detected

Received: April 6, 2023
Revised: April 27, 2023
Published: May 12, 2023

https://doi.org/10.1021/acs.jpca.3c02295
J. Phys. Chem. A 2023, 127, 4483−4491

by mass-selected infrared photodissociation spectroscopy as described in detail previously.[46] The 1064 nm fundamental of a Nd:YAG laser (Continuum, Minilite II) was applied to vaporize a magnesium metal target. The carbonyl complexes were produced in a pulsed supersonic expansion of helium seeded with 10% CO containing a trace of $Fe(CO)_5$ impurity at 0.7−1.2 MPa backing pressure during the laser vaporization process. The cation products were then skimmed and detected by a time-of-flight mass spectrometer (TOFMS). To obtain infrared photodissociation spectra of target cations, the cations were respectively mass-selected, decelerated, and irradiated by a tunable infrared laser. The dissociation laser was generated from an OPO/OPA system (Laser Vision) pumped by a Nd:YAG laser (Continuum Surelite EX). The laser energy is about 0.5−1.0 mJ/pulse in the range of 1600−2280 cm^{-1}. After laser irradiation, the dissociated fragment cations together with undissociated parent cations were reaccelerated and detected by a second TOFMS. Monitoring the dissociation efficiency as a function of laser wavenumber gave the infrared spectrum of the complex. The wavenumber was scanned in steps of 2 cm^{-1} and the dissociation efficiency was averaged over 300 laser shots per step. The wavenumber was calibrated by absorption spectrum of carbon monoxide.

Quantum chemical calculations were carried out to confirm the geometric and electronic structures of the target complexes. Equilibrium geometry optimizations and vibrational frequency simulations were performed at the B3LYP-D3/6-311+G(d) level.[47−50] The harmonic vibrational frequencies were scaled by a factor of 0.969, which is obtained from the ratio of experimental stretching frequency of 2143 cm^{-1} for CO and the calculated value of 2213 cm^{-1}. All calculations were performed using the Gaussian 09 program.[51] To better understand the chemical bonding in the complexes, energy decomposition analysis with natural orbitals of chemical valence (EDA-NOCV)[52,53] was carried out. The instantaneous interaction energy (ΔE_{int}) between two fragments of a molecule is decomposed into three main components: the Pauli repulsion energy (ΔE_{Pauli}), the quasi-classical electrostatic interaction energy (ΔE_{elstat}) and the orbital interaction energy (ΔE_{orb}). The total ΔE_{orb} is further partitioned into several pairwise contributions of the orbital interactions, clarifying the dominant covalent interactions and the orbitals involved. The EDA-NOCV bonding analyses were performed at the PBE/TZ2P level with the ADF 2014 program package[54] using the geometries optimized at the B3LYP-D3/6-311+G(d) level.

■ RESULTS AND DISCUSSION

Figure 1 shows the mass spectrum of the carbonyl cation complexes produced by pulsed laser vaporization of a pure magnesium metal target in an expansion of helium seeded with 10% CO containing trace of $Fe(CO)_5$ impurity. Besides the peaks due to mononuclear magnesium carbonyl complexes $Mg(CO)_n^+$ (n = 2−4), mass peaks due to heteronuclear magnesium−iron carbonyl complexes $MgFe(CO)_n^+$ (n = 4−9) are observed. The mass peaks of $MgFe(CO)_9^+$ remain intense under different experimental conditions while the signals of the $MgFe(CO)_n^+$ ($n \geq 10$) complexes are hardly observed, suggesting that the $MgFe(CO)_9^+$ complex is a coordinatively saturated species.

The heteronuclear complexes $MgFe(CO)_n^+$ (n = 4−9) are each mass-selected and subjected to infrared photodissociation. Each complex dissociates via the loss of a CO ligand in the carbonyl stretching frequency region. The resulting

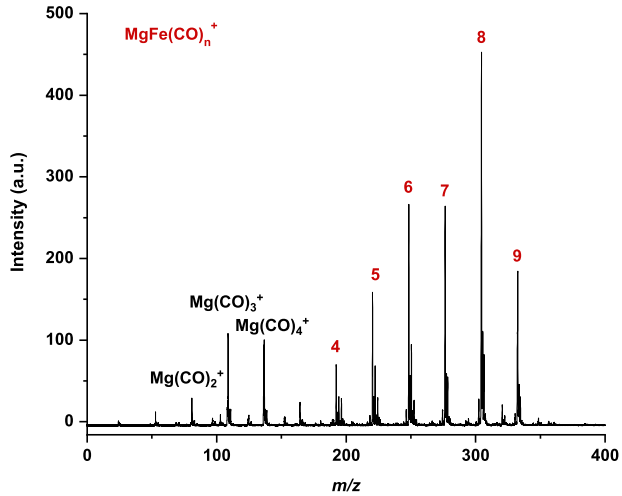

Figure 1. Mass spectrum of the heteronuclear carbonyl cation complexes produced by pulsed laser vaporization of a magnesium target in an expansion of helium seeded by 10% carbon monoxide with trace of $Fe(CO)_5$ impurity.

infrared photodissociation spectra are shown in Figure 2. The $MgFe(CO)_4^+$ complex dissociates quite inefficiently even

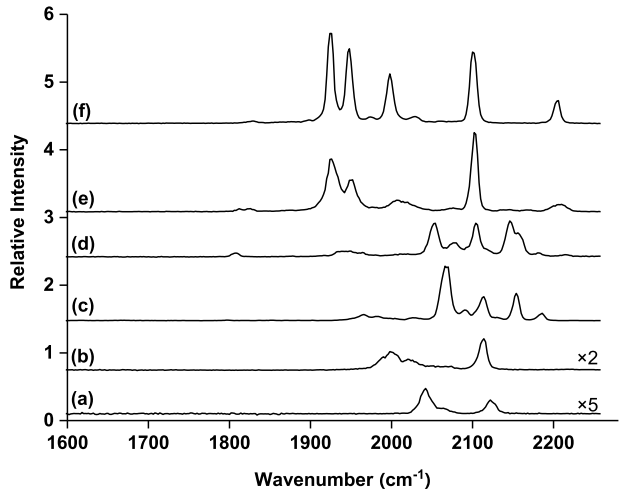

Figure 2. Infrared photodissociation spectra of (a) $MgFe(CO)_4^+$, (b) $MgFe(CO)_5^+$, (c) $MgFe(CO)_6^+$, (d) $MgFe(CO)_7^+$, (e) $MgFe(CO)_8^+$, and (f) $MgFe(CO)_9^+$ in the carbonyl stretching frequency region.

under focused IR laser irradiation (2% at 2043 cm^{-1}). The $MgFe(CO)_n^+$ (n = 5−9) complexes all exhibit appreciable dissociation efficiency under unfocused IR laser irradiation (>5%), indicating relatively weak metal−CO bonding. For the small n = 4−6 complexes, no bands below 1900 cm^{-1} are observed, indicating that all the carbonyl ligands are terminally bonded. In contrast, weak bands below 1900 cm^{-1} are observed for the larger n = 7−9 complexes, suggesting the involvement of bridge bonded carbonyl ligands. No band is observed in the tagged CO stretching frequency region (~2160 cm^{-1}) in the spectrum of $MgFe(CO)_9^+$, indicating that all the CO ligands are chemically bonded.[55−57]

Quantum chemical calculations are performed to validate the experimental assignments and to determine the structures of the heteronuclear magnesium−iron carbonyl complexes. The optimized geometries, relative energies and simulated IR spectra calculated at the B3LYP-D3/6-311+G(d) level for

https://doi.org/10.1021/acs.jpca.3c02295
J. Phys. Chem. A 2023, 127, 4483−4491

different isomers of $MgFe(CO)_n^+$ (n = 4−9) are shown in Figures S1−S6, respectively. The simulated IR spectra are compared to the experimental ones in Figures 3−8, respectively. The most stable structure of each complex is calculated to have a doublet ground state.

For the $MgFe(CO)_4^+$ complex, the first two lowest-lying isomers are both Mg−Fe bonded with a bare Mg atom bonded to a $Fe(CO)_4$ fragment. The first isomer possesses C_{4v} symmetry with the Mg atom coordinated to a near planar $Fe(CO)_4$ fragment. The second isomer has C_s symmetry, which is predicted to be 1.2 kcal·mol^{-1} less stable than the first isomer. The third and fourth isomers (Figure S1 in Supporting Information) lie more than 16 kcal·mol^{-1} higher in energy than the most stable isomer. The simulated spectra of the first two lowest-lying isomers are compared to the experimental spectrum in Figure 3. The results suggest that the

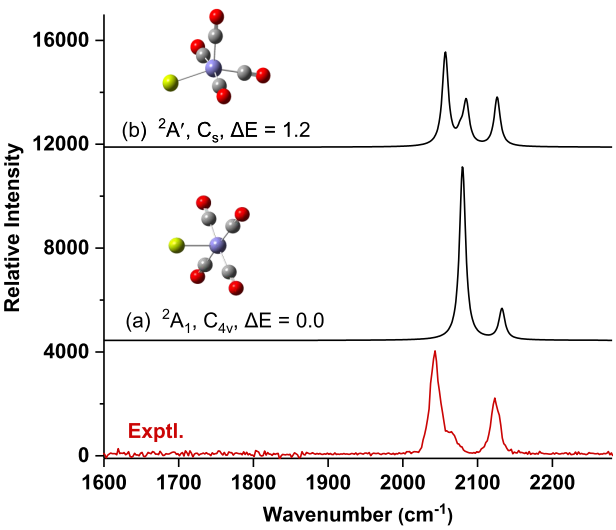

Figure 3. Calculated structures and relative energies (kcal·mol^{-1}) of the first two lowest-lying isomers of $MgFe(CO)_4^+$ at the B3LYP-D3/6-311+G(d) level of theory. Color codes for atoms: red, O; gray, C; purple, Fe; green, Mg. Their simulated IR spectra are compared to the experimental spectrum (in red). The simulated spectra were obtained from scaled (0.969) harmonic vibrational frequencies by applying the Lorentzian line shape function with a 5 cm^{-1} full-width-at-half-maximum.

experimentally observed $MgFe(CO)_4^+$ complex possesses the second structure with Mg−Fe bonded C_s symmetry. However, the coexistence of the first structure cannot be ruled out.

Six low-lying isomers are predicted for $MgFe(CO)_5^+$, all in the doublet ground state, as shown in Figure S2. The most stable isomer has a C_{4v} structure with a bare Mg atom coordinated axially to a C_{4v} symmetric $Fe(CO)_5$ fragment. The second isomer has C_{2v} symmetry with a bare Mg atom coordinated to an equatorial CO ligand of the $Fe(CO)_5$ fragment with D_{3h} symmetry in forming a linear bridging CO ligand. This isomer is predicted to be 3.7 kcal·mol^{-1} higher in energy than the most stable structure. The third lowest-lying isomer has a Mg−Fe bonded structure with one CO ligand terminally bonded on Mg and four CO ligands terminally bonded on Fe. This structure is 7.5 kcal·mol^{-1} higher in energy than the most stable isomer. The fourth isomer also contains a linear bridging CO ligand, which can be regarded as being formed by a bare Mg atom coordinated to an axial CO ligand of the $Fe(CO)_5$ fragment with D_{3h} symmetry. The fifth isomer can be regarded as being formed via adding an additional CO ligand to the Mg center of the most stable isomer of $MgFe(CO)_4^+$. The sixth isomer can be regarded as being formed between a $Mg(CO)_2$ fragment and a $Fe(CO)_3$ fragment. The last three isomers are calculated to lie 8.9, 10.2, and 24.8 kcal·mol^{-1} above the most stable isomer. The simulated spectra of the first three lowest-lying isomers are compared to the experimental spectrum in Figure 4. The

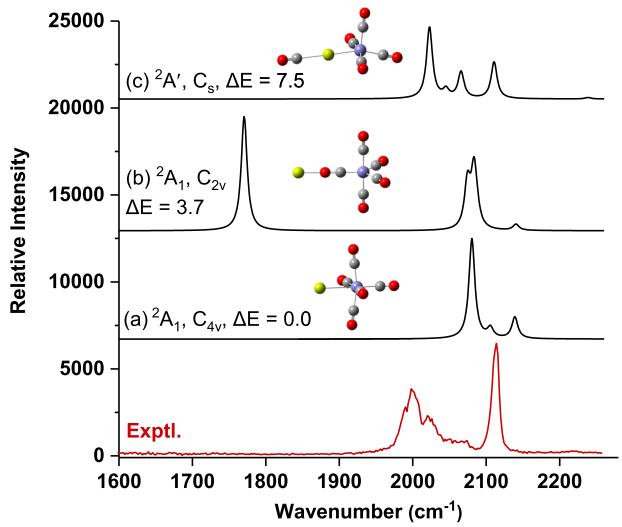

Figure 4. Calculated structures and relative energies (kcal·mol^{-1}) of the first three lowest-lying isomers of $MgFe(CO)_5^+$ at the B3LYP-D3/6-311+G(d) level of theory. Color codes for atoms: red, O; gray, C; purple, Fe; green, Mg. Their simulated IR spectra are compared to the experimental spectrum (in red). The simulated spectra were obtained from scaled (0.969) harmonic vibrational frequencies by applying the Lorentzian line shape function with a 5 cm^{-1} full-width-at-half-maximum.

second structure with a linear bridging CO ligand can clearly be ruled out. The simulated spectrum of the third isomer matches the experimental spectrum, suggesting that the experimentally observed $MgFe(CO)_5^+$ complex possesses the $[(OC)Mg{-}Fe(CO)_4]^+$ structure, which can be regarded as being formed via adding an additional CO ligand to the Mg center of the experimentally observed $MgFe(CO)_4^+$ complex. The experimental spectrum is quite broad, and the first structure most likely coexists.

Four low-lying isomers are predicted for $MgFe(CO)_6^+$, as shown in Figure S3. The most stable isomer has C_s symmetry, which can be viewed as being built from the most stable C_{4v} structure of $MgFe(CO)_5^+$ by adding the sixth CO to the Mg center. The second structure is predicted to have a $[(OC)_2Mg{-}Fe(CO)_4]^+$ structure with C_s symmetry. It is predicted to be only 0.5 kcal·mol^{-1} higher in energy than the most stable structure. The third and fourth structures both involve a linear bridging CO ligand, which can be viewed as being built from the second and fourth stable structures of $MgFe(CO)_5^+$ by adding the sixth CO on the Mg center. These two structures are predicted to be 1.4 and 6.3 kcal·mol^{-1} higher in energy than the most stable structure. The simulated spectra for the first three lowest-lying isomers are compared to the experimental spectrum in Figure 5. The spectrum of the first isomer fits the experimental spectrum above 2050 cm^{-1}

https://doi.org/10.1021/acs.jpca.3c02295
J. Phys. Chem. A 2023, 127, 4483−4491

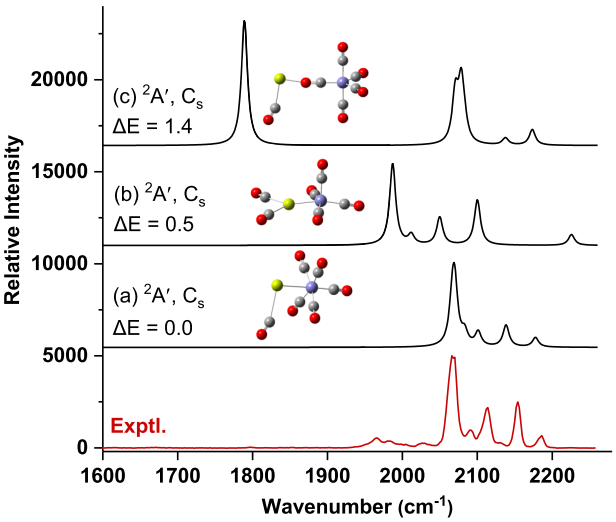

Figure 5. Calculated structures and relative energies (kcal·mol^{-1}) of the first three lowest-lying isomers of $MgFe(CO)_6^+$ at the B3LYP-D3/6-311+G(d) level of theory. Color codes for atoms: red, O; gray, C; purple, Fe; green, Mg. Their simulated IR spectra are compared to the experimental spectrum. The simulated spectra were obtained from scaled (0.969) harmonic vibrational frequencies by applying the Lorentzian line shape function with a 5 cm^{-1} full-width-at-half-maximum.

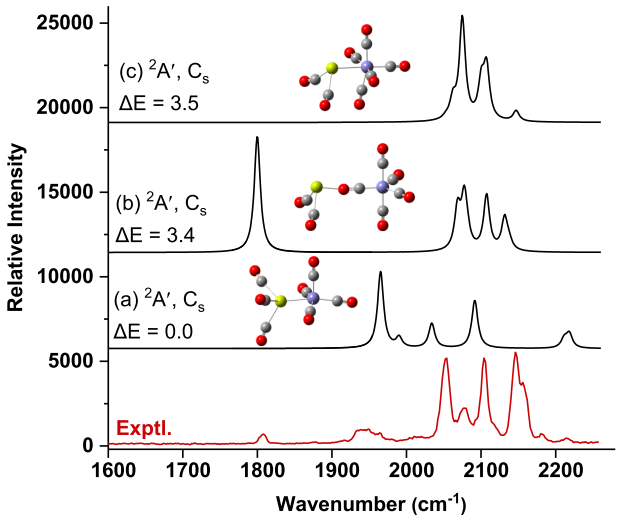

Figure 6. Calculated structures and relative energies (kcal·mol^{-1}) of the first three lowest-lying isomers of $MgFe(CO)_7^+$ at the B3LYP-D3/6-311+G(d) level of theory. Color codes for atoms: red, O; gray, C; purple, Fe; green, Mg. Their simulated IR spectra are compared to the experimental spectrum. The simulated spectra were obtained from scaled (0.969) harmonic vibrational frequencies by applying the Lorentzian line shape function with a 5 cm^{-1} full-width-at-half-maximum.

quite well, indicating that the experimentally observed $MgFe(CO)_6^+$ complex is dominated by the $[(OC)Mg{-}Fe(CO)_5]^+$ structure. As shown in Figure 5, relatively weak bands below 2050 cm^{-1} (1966, 1984, and 2026 cm^{-1}) are also observed in the experimental spectrum, which can be attributed to the second isomer.

Seven low-lying isomers are found starting with various possible geometries of $MgFe(CO)_7^+$, and the results are shown in Figure S4. The most stable structure is predicted to have a $[(OC)_3Mg{-}Fe(CO)_4]^+$ structure with C_s symmetry, which can be viewed as being built from the second most stable structure of $MgFe(CO)_6^+$ by adding the seventh CO to the Mg center. The second lowest-lying isomer possesses a $[(OC)_2Mg{-}OC{-}Fe(CO)_4]^+$ structure involving a linear bridging carbonyl ligand. The third isomer has a $[(OC)_2Mg{-}Fe(CO)_5]^+$ structure with C_s symmetry. The second and third structures are predicted to be 3.4 and 3.5 kcal·mol^{-1} higher in energy than the most stable isomer. The other four isomers lie above the first isomer by 4.6, 8.1, 9.4, and 12.4 kcal·mol^{-1}, respectively. Comparison of the simulated and experimental spectra (Figure 6) indicates that the $MgFe(CO)_7^+$ complex is a mixture involving more than one isomer. The observation of a band around 1950 cm^{-1} indicates the involvement of the $[(CO)_3Mg{-}Fe(CO)_4]^+$ structure with a Mg−Fe bond. The observation of a band centered at 1808 cm^{-1} confirms the involvement of the $[(OC)_2Mg{-}OC{-}Fe(CO)_4]^+$ structure possessing a linear bridging CO ligand.

Eight stable isomers are found for the $MgFe(CO)_8^+$ complex, as shown in Figure S5. The most stable isomer possesses a metal−metal bonded $[(CO)_4Mg{-}Fe(CO)_4]^+$ structure. The second isomer is predicted to have a $[(OC)_3Mg{-}OC{-}Fe(CO)_4]^+$ structure involving a linear bridging carbonyl ligand, which is 2.5 kcal·mol^{-1} less stable than the first isomer. The third isomer has a Mg−Fe bonded $[(OC)_3Mg{-}Fe(CO)_5]^+$ structure without symmetry. It is predicted to be 4.0 kcal·mol^{-1} above the most stable isomer.

The simulated IR spectra of the three lowest-lying isomers are shown in Figure 7. The simulated spectrum of the most stable

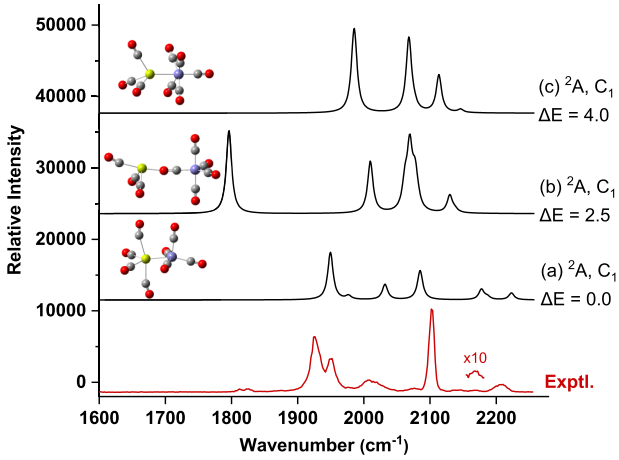

Figure 7. Calculated structures and relative energies (kcal·mol^{-1}) of the first three lowest-lying isomers of $MgFe(CO)_8^+$ at the B3LYP-D3/6-311+G(d) level of theory. Color codes for atoms: red, O; gray, C; purple, Fe; green, Mg. Their simulated IR spectra are compared to the experimental spectrum. The simulated spectra were obtained from scaled (0.969) harmonic vibrational frequencies by applying the Lorentzian line shape function with a 5 cm^{-1} full-width-at-half-maximum.

isomer matches well with the major features in the experimental spectrum, indicating that the $MgFe(CO)_8^+$ complex possesses the Mg−Fe bonded $[(CO)_4Mg{-}Fe{-}(CO)_4]^+$ structure. The observation of a very weak band around 1820 cm^{-1} implies the involvement of the $[(OC)_3Mg{-}OC{-}Fe(CO)_4]^+$ structure with a linear bridging carbonyl ligand as well.

Six low-lying isomers are predicted for $MgFe(CO)_9^+$, which are shown in Figure S6. The first isomer has a $[(OC)_4Mg{-}$

https://doi.org/10.1021/acs.jpca.3c02295
J. Phys. Chem. A 2023, 127, 4483−4491

OC−Fe(CO)$_4$]$^+$ structure with C_{2v} symmetry involving a linear bridging carbonyl ligand. The second isomer possesses a Mg−Fe bonded [(CO)$_4$Mg−Fe(CO)$_5$]$^+$ structure with C_{4v} symmetry, which lies 2.1 kcal·mol^{-1} above the first structure. The third isomer has a [(OC)$_5$Mg−Fe(CO)$_4$]$^+$ structure with C_s symmetry, which is 3.9 kcal·mol^{-1} higher in energy than the first isomer. As shown in Figure 8, the simulated spectrum of

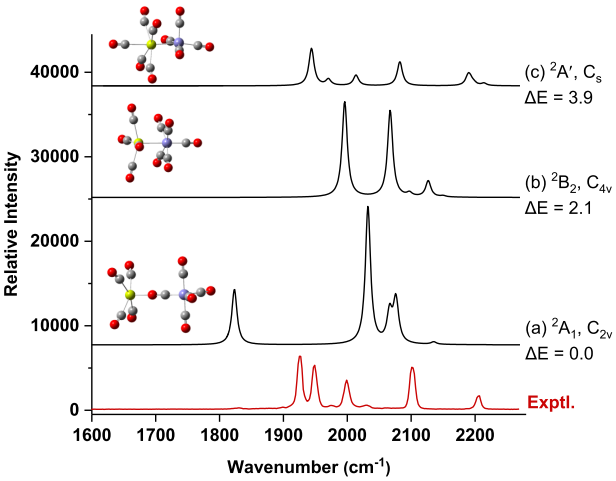

Figure 8. Calculated structures and relative energies (kcal·mol^{-1}) of the first three lowest-lying isomers of MgFe(CO)$_9^+$ at the B3LYP-D3/6-311+G(d) level of theory. Color codes for atoms: red, O; gray, C; purple, Fe; green, Mg. Their simulated IR spectra are compared to the experimental spectrum. The simulated spectra were obtained from scaled (0.969) harmonic vibrational frequencies by applying Lorentzian line shape function with a 5 cm^{-1} full-width-at-half-maximum.

the third isomer matches well with the experimental spectrum, indicating that the coordinatively saturated MgFe(CO)$_9^+$ complex possesses the [(CO)$_5$Mg−Fe(CO)$_4$]$^+$ structure containing a Mg−Fe bond. A very weak band at 1829 cm^{-1} is also observed in the experimental spectrum, suggesting that the first structure is also presented in the experiment.

Infrared photodissociation spectroscopy in combination with theoretical calculations confirm that the MgFe(CO)$_n^+$ (n = 4−9) complexes each contain more than one isomer. The small complexes (n = 4−6) possess the Mg−Fe bonded structures with all the carbonyl ligands terminally bonded. Both the [(OC)$_{n-4}$Mg−Fe(CO)$_4$]$^+$ and [(OC)$_{n-5}$Mg−Fe(CO)$_5$]$^+$ isomers are presented for the n = 5, 6 complexes. For the larger complexes with n > 6, the [(OC)$_{n-4}$Mg−Fe(CO)$_4$]$^+$ structure is the major isomer experimentally observed. In addition, the [(OC)$_{n-5}$Mg−OC−Fe(CO)$_4$]$^+$ isomer involving a linear bridging carbonyl ligand is also characterized. Table 1 shows the comparison of the experimental and calculated carbonyl stretching frequencies of the MgFe(CO)$_n^+$ (n = 4−9) complexes. The values in bold correspond to the terminal CO ligands coordinated on the Mg center. These values for the [(OC)$_{n-4}$Mg−Fe(CO)$_4$]$^+$ structures retain close to 2200 cm^{-1}, significantly blue-shifted from that of free CO at 2143 cm^{-1}, indicating that the corresponding CO ligands are coordinated on the positively charged Mg centers.

Table 2 shows the Mg−Fe bond distances, bond dissociation energies, and NPA charges of the Mg(CO)$_{n-4}$ and Fe(CO)$_4$ fragments in the [(CO)$_{n-4}$Mg−Fe(CO)$_4$]$^+$ isomers (n = 4−9).

Table 1. Observed and Calculated (B3LYP-D3/6-311+G(d) Level) Carbonyl Stretching Frequencies (in cm^{-1}) of MgFe(CO)$_n^+$ (n = 4−9)[a]

	Exptl		Calcd
MgFe(CO)$_4^+$	2043, 2067, 2123	**4b**	2057, 2078, 2084, 2126
		4a	2079, 2133
MgFe(CO)$_5^+$	1998, 2020, 2074, 2114, **2218**	**5c**	2023, 2045, 2067, 2110, **2238**
		5a	2080, 2106, 2139
MgFe(CO)$_6^+$	2066, 2090, 2114, 2154, **2186**	**6a**	2069, 2082, 2102, 2139, **2178**
	1966, 1984, 2026, 2130, **2224**	**6b**	1987, 2012, 2049, 2100, **2226**[b]
MgFe(CO)$_7^+$	1944, 1964, 2010, 2078, **2214**	**7a**	1965, 1990, 2034, 2091, **2218**[c]
	1808, 2054, **2104**, **2146**, 2156	**7b**	1799, 2069, 2078, **2108**, **2132**, 2138
MgFe(CO)$_8^+$	1926, 1952, 2010, 2102, **2168**, **2208**	**8a**	1950, 1977, 2032, 2085, **2178**, **2188**, **2223**[b]
	1820, **1976**, **2076**, **2146**	**8b**	1797, **2010**, **2062**, 2070, 2077,[b] **2130**[b]
MgFe(CO)$_9^+$	1925, 1949, 1999, 2101, **2207**	**9c**	1944, 1970, 2014, 2082, **2188−2214**[d]
	1829, **2031**, 2061	**9a**	1824, **2032**,[c] 2067, 2076,[b] 2135, **2144**

[a]The bold values represent or contain the stretching frequencies of the carbonyl ligands coordinated on Mg. [b]Two narrow-spaced lines. [c]Three narrow-spaced lines. [d]Five narrow-spaced lines.

The increase of CO ligands has weak effect on the Mg−Fe bond distances, which vary in a small range of 2.465 to 2.608 Å. These values are quite close to the sum of the single-bond covalent radii of Mg and Fe (Mg + Fe = 2.53 Å),[58] suggesting that the Mg−Fe bonds are all single bonds. The Mg−Fe bond dissociation energies are all close to 40 kcal·mol^{-1} from n = 4 to 9. Natural population analysis shows that the Fe(CO)$_4$ fragment is almost neutral and the positive charge is located on the Mg center in the MgFe(CO)$_4^+$ complex (Table 2). The positive charge on the Mg(CO)$_{n-4}$ fragment increases monotonically with the number of coordinated CO ligands on Mg increasing, indicating electron transfer from Mg to the Fe(CO)$_4$ fragment. Figure 9 shows the singly occupied molecular orbital (SOMO) and the highest doubly occupied molecular orbital (HOMO−1) of the coordinatively saturated MgFe(CO)$_9^+$ complex, and those of the [(CO)$_{n-4}$Mg−Fe(CO)$_4$]$^+$ (n = 4−8) complexes are shown in Figure S7. For each complex, the unpaired electron is mainly located at the Fe center. The HOMO−1 is a σ-type Mg−Fe bonded orbital.

Energy decomposition analysis with natural orbital for chemical valence (EDA-NOCV) is performed to get deep insight into the Mg−Fe bonding in these complexes. The bonding situation in the coordinatively saturated MgFe(CO)$_9^+$ complex is investigated using either Mg(CO)$_5^+$ in the doublet ground state and Fe(CO)$_4$ in the triplet ground state or Mg(CO)$_5^{2+}$ in the singlet ground state and Fe(CO)$_4^-$ in the doublet ground state as interacting fragments. The former describes the HOMO−1 as electron-sharing σ bonding while the latter describes it as (CO)$_5$Mg^{2+}←Fe(CO)$_4^-$ dative bonding. The numerical results of the EDA-NOCV calculations for MgFe(CO)$_9^+$ are shown in Table S1. Since the description using the fragments Mg(CO)$_5^+$ (D) and Fe(CO)$_4$ (T) leads to a smaller value for the orbital interaction ΔE_{orb}, this description should be chosen for analyzing the bonding situation.[59,60] The numerical results (Table 3) indicate that the

https://doi.org/10.1021/acs.jpca.3c02295
J. Phys. Chem. A 2023, 127, 4483−4491

Table 2. Mg−Fe Bond Distances (in Å), Dissociation Energies (in kcal·mol^{-1}), and Natural Charges of the $[(CO)_{n-4}Mg-Fe(CO)_4]^+$ (n = 4−9) Isomers

complex structure	Mg−Fe bond distance	Mg−Fe bond dissociation energy	NPA group charge			
			$Mg(CO)_{n-4}$	Mg	$Fe(CO)_4$	Fe
4b	2.577	41.0	0.99	0.99	0.01	−1.62
5c	2.494	40.9	1.26	1.11	−0.26	−1.80
6b	2.465	42.5	1.37	1.02	−0.37	−1.84
7a	2.478	42.2	1.38	0.76	−0.38	−1.80
8a	2.520	39.9	1.40	0.55	−0.40	−1.79
9c	2.608	38.1	1.43	0.37	−0.43	−1.78

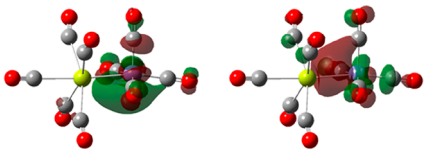

Figure 9. Contours of the singly occupied molecular orbital (SOMO) and the σ-type bonding MO (isosurface = 0.04 au) of the $MgFe(CO)_9^+$ complex.

bonding between the fragments $Mg(CO)_5^+$ and $Fe(CO)_4$ possesses a higher covalent character (59.7%) than electrostatic character (40.3%). The decomposition of ΔE_{orb} into pairwise orbital interactions suggests that the dominant orbital interaction is an σ-type electron-sharing bonding, contributing 80.9% of the covalent interaction. The $\Delta E_{orb(2)}$ and $\Delta E_{orb(3)}$ correspond to two $(CO)_5Mg^+ \leftarrow Fe(CO)_4$ dative π bonding components; both are rather weak, leading to orbital interaction energies of only 3.2 and 3.0 kcal·mol^{-1}. Figure 10 exhibits the deformation densities $\Delta\rho$ and the most relevant associated MOs of the fragments corresponding to these interactions. Therefore, the Mg−Fe bonding in the $MgFe(CO)_9^+$ complex is identified as Mg−Fe electron-sharing σ single bonding.

The σ bonding deserves a more careful investigation. According to Figure 10a, the α term of the deformation densities represents electron migration from $Fe(CO)_4$ (T) to the SOMO of $Mg(CO)_5^+$ (D) while the β term represents the electron migration in an opposite direction. The NOCV eigenvalue $|\nu|$ of the deformation densities indicates the size of charge migration. The $|\nu_\beta|$ value is much larger than the $|\nu_\alpha|$ value, suggesting significant electron density migration from the SOMO of $Mg(CO)_5^+$ to $Fe(CO)_4$ during the σ bonding, causing the $Mg(CO)_5$ moiety highly positively charged. The SOMO of $Mg(CO)_5^+$ initially contains some Mg → CO π back-donation character, which is sharply weakened by the electron density migration effect of the electron-sharing σ bonding, resulting in the blue shift of the stretching frequencies of the CO ligands coordinated on the Mg atom.

EDA-NOCV calculations are further performed for the coordinatively unsaturated species $[(CO)_{n-4}Mg-Fe(CO)_4]^+$ (n = 4−8). Considering the positive charge populated on the $Mg(CO)_{n-4}$ (n = 4−8) moieties is smaller than that on the $Mg(CO)_5$ fragment in $MgFe(CO)_9^+$, only the fragments $Mg(CO)_{n-4}^+$ in the doublet ground state and $Fe(CO)_4$ in the triplet ground state are used to study the Mg−Fe bonding. The numerical results are shown in Table 3. The Mg−Fe bonding in $[(CO)_{n-4}Mg-Fe(CO)_4]^+$ (n = 4−8) should all be identified as Mg−Fe electron-sharing σ single bond. The instantaneous interaction energies (ΔE_{int}) for the Mg−Fe bonding in $[(CO)_{n-4}Mg-Fe(CO)_4]^+$ (n = 4−9) are all calculated to be close to 50 kcal·mol^{-1}. Although ΔE_{int} and bond dissociation energy have different physical meanings, they both indicate that the Mg−Fe bonding is hardly strengthened or weakened due to CO coordination to the Mg center.

Figure S8 shows the deformation densities $\Delta\rho$ and the relevant associated MOs of the fragments corresponding to the σ-type orbital interactions for $[(OC)_{n-4}Mg-Fe(CO)_4]^+$ (n = 4−9). With the increase of CO ligands coordinated on the Mg atom, the $|\nu_\alpha|$ decreases and the $|\nu_\beta|$ increases gradually, suggesting more electron density migration from Mg to Fe. The Mg−Fe σ bonding is almost nonpolar in $MgFe(CO)_4^+$ while it is apparently polarized to Fe in the larger complexes according to the $|\nu|$ values. Such an electron density migration tendency is in accord with the natural population analysis listed in Table 2. Accordingly, the valence of Mg can be recognized as +I in $MgFe(CO)_4^+$ while it is altered to +II in the larger $MgFe(CO)_n^+$ (n = 5−9) complexes. The Mg(+I)−Fe(0) bonding transforms to Mg(+II)−Fe(−I) bonding due to CO

Table 3. EDA-NOCV Results of $[(CO)_{n-4}Mg-Fe(CO)_4]^+$ (n = 4−9) at the PBE/TZ2P Level Using the Fragments $Mg(CO)_{n-4}^+$ in the Doublet State (D) and $Fe(CO)_4$ in the Triplet State (T) (Energy Values in kcal·mol^{-1})

Energy	$MgFe(CO)_4^+$	$MgFe(CO)_5^+$	$MgFe(CO)_6^+$	$MgFe(CO)_7^+$	$MgFe(CO)_8^+$	$MgFe(CO)_9^+$
ΔE_{int}	−52.3	−53.2	−54.0	−52.0	−50.1	−49.1
ΔE_{Pauli}	23.7	52.1	67.4	72.3	73.1	73.1
ΔE_{elstat} [a]	−16.6 (21.8%)	−39.3 (37.3%)	−50.8 (41.8%)	−51.2 (41.2%)	−49.5 (40.2%)	−49.2 (40.3%)
ΔE_{orb} [a]	−59.4 (78.2%)	−66.0 (62.7%)	−70.6 (58.2%)	−73.1 (58.8%)	−73.7 (59.8%)	−73.0 (59.7%)
$\Delta E_{orb(1,\sigma)}$ [b]	−41.5 (69.8%)	−48.1 (72.9%)	−53.5 (75.8%)	−56.6 (77.5%)	−57.8 (78.4%)	−59.1 (80.9%)
$\Delta E_{orb(2,\pi)}$ [b]	−4.1 (6.9%)	−4.4 (6.6%)	−4.4 (6.3%)	−4.3 (5.9%)	−4.2 (5.7%)	−3.2 (4.4%)
$\Delta E_{orb(3,\pi)}$ [b]	−3.6 (6.1%)	−4.5 (6.8%)	−4.3 (6.1%)	−4.1 (5.6%)	−3.8 (5.2%)	−3.0 (4.1%)
$\Delta E_{orb(rest)}$ [b]	−10.2 (17.1%)	−9.0 (13.7%)	−8.3 (11.8%)	−8.0 (11.0%)	−7.9 (10.7%)	−7.7 (10.6%)

[a]The values in parentheses give the percentage contribution to the total attractive interactions $\Delta E_{elstat} + \Delta E_{orb}$. [b]The values in parentheses give the percentage contribution to the total orbital interactions ΔE_{orb}.

https://doi.org/10.1021/acs.jpca.3c02295
J. Phys. Chem. A 2023, 127, 4483−4491

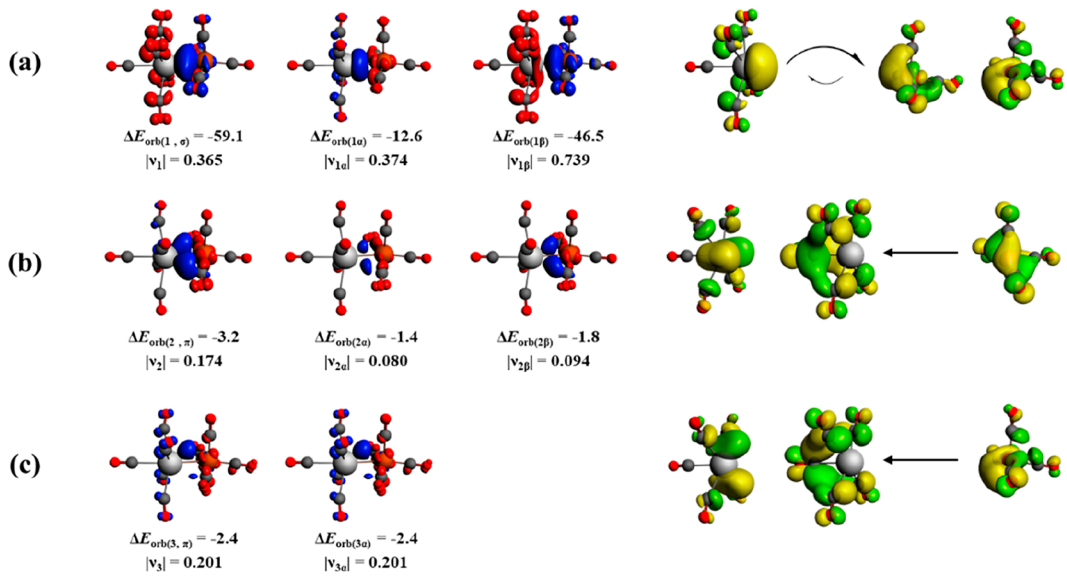

Figure 10. Plot of the deformation densities $\Delta\rho$ (isovalue = 0.002 au for $\Delta\rho_1$ and isovalue = 0.0006 au for $\Delta\rho_2$, $\Delta\rho_3$) of the three most important pairwise orbital interactions (see Table 3) and shape of the most relevant associated MOs of the fragments for $MgFe(CO)_9^+$. The direction of the charge flow is red → blue. Energy values are given in kcal·mol^{-1}.

coordinating on the Mg center. Although the Mg → CO π back-donation character in the free $Mg(CO)_{n-4}^+$ complexes increases from n = 6−9 according to the CO $2p_\pi$ contributions shown in Table S2 due to increased sp hybridization, the increased electron transfer from Mg to Fe causes a steady decrease of the Mg → CO π back-donation character with the number of CO ligands on Mg increasing. This results in very small shifts of the stretching frequencies of the corresponding CO ligands from n = 6−9.

CONCLUSIONS

Heteronuclear magnesium−iron carbonyl cation complexes $MgFe(CO)_n^+$ (n = 4−9) are prepared in the gas phase. Mass-selected infrared photodissociation spectroscopy combined with theoretical calculations confirm that $MgFe(CO)_9^+$ is a coordinatively saturated complex. Each complex is characterized to contain more than one isomer. The small complexes (n = 4−6) possess the Mg−Fe bonded $[(OC)_{n-4}Mg-Fe(CO)_4]^+$ and/or $[(OC)_{n-5}Mg-Fe(CO)_5]^+$ structures with all the carbonyl ligands terminally bonded. For the larger complexes with n = 7−9, the $[(OC)_{n-4}Mg-Fe(CO)_4]^+$ structure is the major isomer experimentally observed. In addition, the $[(OC)_{n-5}Mg-OC-Fe(CO)_4]^+$ isomer involving a linear bridging carbonyl ligand is also characterized. Bonding analyses indicate that each $[(OC)_{n-4}Mg-Fe(CO)_4]^+$ complex contains a Mg−Fe electron-sharing σ bond. The metal−metal bond is described as a Mg(+I)−Fe(0) bond in $MgFe(CO)_4^+$ and as a Mg(+II)−Fe(−I) bond in the larger n = 5−9 complexes due to electron transfer from Mg to Fe promoted by CO coordination on the Mg center.

ASSOCIATED CONTENT

Supporting Information

The Supporting Information is available free of charge at https://pubs.acs.org/doi/10.1021/acs.jpca.3c02295.

Calculated structures and relative energies, the contours of molecular orbitals, Plot of the deformation densities, the EDA-NOCV results, AO contributions, and coordinates and energies of the $MgFe(CO)_n^+$ (n = 4−9) complexes (PDF)

AUTHOR INFORMATION

Corresponding Author

Mingfei Zhou − *Collaborative Innovation Center of Chemistry for Energy Materials, Department of Chemistry, Shanghai Key Laboratory of Molecular Catalysts and Innovative Materials, Fudan University, Shanghai 200438, China;* orcid.org/0000-0002-1915-6203; Email: mfzhou@fudan.edu.cn

Authors

Xiaoyang Jin − *Collaborative Innovation Center of Chemistry for Energy Materials, Department of Chemistry, Shanghai Key Laboratory of Molecular Catalysts and Innovative Materials, Fudan University, Shanghai 200438, China*

Yangyu Zhou − *Collaborative Innovation Center of Chemistry for Energy Materials, Department of Chemistry, Shanghai Key Laboratory of Molecular Catalysts and Innovative Materials, Fudan University, Shanghai 200438, China*

Guanjun Wang − *Collaborative Innovation Center of Chemistry for Energy Materials, Department of Chemistry, Shanghai Key Laboratory of Molecular Catalysts and Innovative Materials, Fudan University, Shanghai 200438, China;* orcid.org/0000-0002-3265-7192

Complete contact information is available at: https://pubs.acs.org/10.1021/acs.jpca.3c02295

Notes

The authors declare no competing financial interest.

ACKNOWLEDGMENTS

The work was financially supported by the National Natural Science Foundation of China (Grant number 21688102).

REFERENCES

(1) Powers, I. G.; Uyeda, C. Metal−Metal Bonds in Catalysis. *ACS Catal.* **2017**, *7*, 936−958.

(2) Berry, J. F.; Lu, C. C. Metal-Metal Bonds: From Fundamentals to Applications. *Inorg. Chem.* **2017**, *56*, 7577−7581.
(3) Chipman, J. A.; Berry, J. F. Paramagnetic Metal-Metal Bonded Heterometallic Complexes. *Chem. Rev.* **2020**, *120*, 2409−2447.
(4) Wang, Q.; Brooks, S. H.; Liu, T.; Tomson, N. C. Tuning Metal-Metal Interactions for Cooperative Small Molecule Activation. *Chem. Commun.* **2021**, *57*, 2839−2853.
(5) Lindahl, P. A. Metal-Metal Bonds in Biology. *J. Inorg. Biochem.* **2012**, *106*, 172−178.
(6) Kondinski, A. Metal-Metal Bonds in Polyoxometalate Chemistry. *Nanoscale* **2021**, *13*, 13574−13592.
(7) Cotton, F. A.; Murillo, C. A.; Walton, R. A. *Multiple Bonds Between Metal Atoms*, 3rd ed.; Springer Science and Business Media: New York, 2005.
(8) Nguyen, T.; Sutton, A. D.; Brynda, M.; Fettinger, J. C.; Long, G. J.; Power, P. P. Synthesis of a Stable Compound with Fivefold Bonding between Two Chromium(I) Centers. *Science* **2005**, *310*, 844−847.
(9) Liddle, S. T. *Molecular Metal-Metal Bonds*; Wiley-VCH Verlag GmbH: Weinheim, 2015.
(10) Wilson, R. J.; Lichtenberger, N.; Weinert, B.; Dehnen, S. Intermetalloid and Heterometallic Clusters Combining p-Block (Semi)Metals with d- or f-Block Metals. *Chem. Rev.* **2019**, *119*, 8506−8554.
(11) Fischer, R. C.; Power, P. P. π-Bonding and the Lone Pair Effect in Multiple Bonds Involving Heavier Main Group Elements: Developments in the New Millennium. *Chem. Rev.* **2010**, *110*, 3877−3923.
(12) Balázs, G.; Gregoriades, L. J.; Scheer, M. Triple Bonds Between Transition Metals and the Heavier Elements of Groups 14 and 15. *Organometallics* **2007**, *26*, 3058−3075.
(13) Zhang, X. X.; Popov, I. A.; Lundell, K. A.; Wang, H. P.; Mu, C. N.; Wang, W.; Schnoeckel, H.; Boldyrev, A. I.; Bowen, K. H. Realization of an Al≡Al Triple Bond in the Gas-Phase $Na_3Al_2^-$ Cluster via Double Electronic Transmutation. *Angew. Chem., Int. Ed.* **2018**, *57*, 14060−14064.
(14) Wang, J. Q.; Chi, C. X.; Hu, H. S.; Meng, L. Y.; Luo, M. B.; Li, J.; Zhou, M. F. Triple Bonds between Iron and Heavier Group 15 Elements in $AFe(CO)_3^-$ (A = As, Sb, Bi) Complexes. *Angew. Chem., Int. Ed.* **2018**, *57*, 542−546.
(15) Chi, C. X.; Wang, J. Q.; Hu, H. S.; Zhang, Y. Y.; Li, W. L.; Meng, L. Y.; Luo, M. B.; Zhou, M. F.; Li, J. Quadruple Bonding Between Iron and Boron in the $BFe(CO)_3^-$ Complex. *Nat. Commun.* **2019**, *10*, 4713.
(16) Merritt, J. M.; Bondybey, V. E.; Heaven, M. C. Beryllium Dimer-Caught in the Act of Bonding. *Science* **2009**, *324*, 1548−1551.
(17) Heaven, M. C.; Bondybey, V. E.; Merritt, J. M.; Kaledin, A. L. The Unique Bonding Characteristics of Beryllium and the Group IIA Metals. *Chem. Phys. Lett.* **2011**, *506*, 1−14.
(18) Chen, M. H.; Zhang, Q. N.; Zhou, M. F.; Andrada, D. M.; Frenking, G. Carbon Monoxide Bonding with BeO and $BeCO_3$: Surprisingly High CO Stretching Frequency of $OCBeCO_3$. *Angew. Chem., Int. Ed.* **2015**, *54*, 124−128.
(19) Arrowsmith, M.; Braunschweig, H.; Celik, M. A.; Dellermann, T.; Dewhurst, R. D.; Ewing, W. C.; Hammond, K.; Kramer, T.; Krummenacher, I.; Mies, J.; et al. Neutral Zero-Valent s-Block Complexes with Strong Multiple Bonding. *Nat. Chem.* **2016**, *8*, 890−894.
(20) Naglav, D.; Buchner, M. R.; Bendt, G.; Kraus, F.; Schulz, S. Off the Beaten Track-A Hitchhiker's Guide to Beryllium Chemistry. *Angew. Chem., Int. Ed.* **2016**, *55*, 10562−10576.
(21) Perera, L. C.; Raymond, O.; Henderson, W.; Brothers, P. J.; Plieger, P. G. Advances in Beryllium Coordination Chemistry. *Coord. Chem. Rev.* **2017**, *352*, 264−290.
(22) Chi, C.; Pan, S.; Meng, L.; Luo, M.; Zhao, L.; Zhou, M.; Frenking, G. Alkali Metal Covalent Bonding in Nickel Carbonyl Complexes $ENi(CO)_3^-$. *Angew. Chem., Int. Ed.* **2019**, *58*, 1732−1738.
(23) Chapple, P. M.; Cartron, J.; Hamdoun, G.; Kahlal, S.; Cordier, M.; Oulyadi, H.; Carpentier, J. F.; Saillard, J. Y.; Sarazin, Y. Metal-Metal Bonded Alkaline-Earth Distannyls. *Chem. Sci.* **2021**, *12*, 7098−7114.
(24) Wu, X.; Zhao, L. L.; Jin, J. Y.; Pan, S.; Li, W.; Jin, X. Y.; Wang, G. J.; Zhou, M. F.; Frenking, G. Observation of Alkaline Earth Complexes $M(CO)_8$ (M = Ca, Sr, or Ba) that Mimic Transition Metals. *Science* **2018**, *361*, 912−916.
(25) Wang, Q.; Pan, S.; Wu, Y. B.; Deng, G. H.; Bian, J. H.; Wang, G. J.; Zhao, L. L.; Zhou, M. F.; Frenking, G. Transition-Metal Chemistry of Alkaline-Earth Elements: The Trisbenzene Complexes $M(Bz)_3$ (M = Sr, Ba). *Angew. Chem., Int. Ed.* **2019**, *58*, 17365−17374.
(26) Wang, Q.; Pan, S.; Lei, S. J.; Jin, J. Y.; Deng, G. H.; Wang, G. J.; Zhao, L. L.; Zhou, M. F.; Frenking, G. Octa-Coordinated Alkaline Earth Metal-Dinitrogen Complexes $M(N_2)_8$ (M = Ca, Sr, Ba). *Nat. Commun.* **2019**, *10*, 3375.
(27) Jin, X. Y.; Bai, Y. N.; Zhou, Y. Y.; Wang, G. J.; Zhao, L. L.; Zhou, M. F.; Frenking, G. Highly Coordinated Heteronuclear Calcium−Iron Carbonyl Cation Complexes $[CaFe(CO)_n]^+$ (n = 5−12) with d-d Bonding. *Angew. Chem., Int. Ed.* **2021**, *60*, 13865−13870.
(28) Zhou, M. F.; Frenking, G. The Transition Metal Chemistry of the Heavier Alkaline Earth Atoms Ca, Sr. *Ba. Acc. Chem. Res.* **2021**, *54*, 3071−3082.
(29) Green, S. P.; Jones, C.; Stasch, A. Stable Magnesium(I) Compounds with Mg-Mg Bonds. *Science* **2007**, *318*, 1754−1757.
(30) Jones, C. Open Questions in Low Oxidation State Group 2 Chemistry. *Commun. Chem.* **2020**, *3*, 159−162.
(31) Stasch, A.; Jones, C. Stable Dimeric Magnesium(I) Compounds: From Chemical Landmarks to Versatile Reagents. *Dalton Trans.* **2011**, *40*, 5659−5672.
(32) Bonyhady, S. J.; Jones, C.; Nembenna, S.; Stasch, A.; Edwards, A. J.; McIntyre, G. J. β-Diketiminate-Stabilized Magnesium(I) Dimers and Magnesium(II) Hydride Complexes: Synthesis, Characterization, Adduct Formation, and Reactivity Studies. *Chem.—Eur. J.* **2010**, *16*, 938−955.
(33) Jones, C. Dimeric Magnesium(I) β-Diketiminates: A New Class of Quasi-Universal Reducing Agent. *Nat. Rev. Chem.* **2017**, *1*, No. 0059.
(34) Platts, J. A.; Overgaard, J.; Jones, C.; Iversen, B. B.; Stasch, A. First Experimental Characterization of a Non-Nuclear Attractor in a Dimeric Magnesium(I) Compound. *J. Phys. Chem. A* **2011**, *115*, 194−200.
(35) Rosch, B.; Gentner, T. X.; Eyselein, J.; Langer, J.; Elsen, H.; Harder, S. Strongly Reducing Magnesium(0) Complexes. *Nature* **2021**, *592*, 717−721.
(36) Felkin, H.; Knowles, P. J.; Meunier, B.; Mitschle, A.; Ricard, L.; Weiss, R. Preparation and Crystal-Structure of π-Cyclopentadienyl-1,2-Bis- (Diphenylphosphino) Ethaneironmagnesium Bromide Tris-(Tetrahydrofuran), a Transition-Metal Grignard Reagent. *J. Am. Chem. Soc. Chem. Commun.* **1974**, *2*, 44.
(37) Jonas, K.; Koepe, G.; Kruger, C. Heterometallic Dinuclear Complexes by Ethene Displacement with Grignard Compounds or Diorganomagnesium Compounds. *Angew. Chem., Int. Ed.* **1986**, *25*, 923−925.
(38) Blake, M. P.; Kaltsoyannis, N.; Mountford, P. Synthesis and Reactions of β-Diketiminate-Supported Complexes with Mg−Fe or Yb−Fe Bonds. *Chem. Commun.* **2013**, *49*, 3315−3317.
(39) Hicks, J.; Hoyer, C. E.; Moubaraki, B.; Li Manni, G.; Carter, E.; Murphy, D. M.; Murray, K. S.; Gagliardi, L.; Jones, C. A Two-Coordinate Manganese(0) Complex with an Unsupported Mn-Mg Bond: Allowing Access to Low Coordinate Homo- and Hetero-bimetallic Compounds. *J. Am. Chem. Soc.* **2014**, *136*, 5283−5286.
(40) Hicks, J.; Underhill, E. J.; Kefalidis, C. E.; Maron, L.; Jones, C. A Mixed-Valence Tri-Zinc Complex, [LZnZnZnL] (L = Bulky Amide), Bearing a Linear Chain of Two-Coordinate Zinc Atoms. *Angew. Chem., Int. Ed.* **2015**, *54*, 10000−10004.
(41) Bakewell, C.; Ward, B. J.; White, A. J. P.; Crimmin, M. R. A Combined Experimental and Computational Study on the Reaction of Fluoroarenes with Mg-Mg, Mg-Zn. *Mg-Al and Al-Zn Bonds. Chem. Sci.* **2018**, *9*, 2348−2356.

https://doi.org/10.1021/acs.jpca.3c02295
J. Phys. Chem. A 2023, 127, 4483−4491

(42) Hicks, J.; Juckel, M.; Jones, C. X-ray Crystal Structures of Carbonate and Hydroxide Bridged Mn^{II}/Mg^{II} Heterobimetallic Complexes Formed by Reduction of CO_2 or H_2O by a Mn^0-Mg^{II} Bonded Compound. *Main Group Met. Chem.* **2021**, *44*, 250−255.
(43) Baddour, F. G.; Hyre, A. S.; Guillet, J. L.; Pascual, D.; Lopez-de-Luzuriaga, J. M.; Alam, T. M.; Bacon, J. W.; Doerrer, L. H. Pt-Mg, Pt-Ca, and Pt-Zn Lantern Complexes and Metal-Only Donor-Acceptor Interactions. *Inorg. Chem.* **2017**, *56*, 452−469.
(44) Kelly, J. A.; Gramuller, J.; Gschwind, R. M.; Wolf, R. Low-Oxidation State Cobalt-Magnesium Complexes: Ion-Pairing and Reactivity. *Dalton Trans.* **2021**, *50*, 13985−13992.
(45) Jin, X.; Wang, G.; Zhou, M. Mg(I)-Fe(−II) and Mg(0)-Mg(I) Covalent Bonding in the $Mg_nFe(CO)_4^-$ (n = 1, 2) Anion Complexes: An Infrared Photodissociation Spectroscopic and Theoretical Study. *Phys. Chem. Chem. Phys.* **2023**, *25*, 7697−7703.
(46) Wang, G.; Chi, C.; Xing, X.; Ding, C.; Zhou, M. A Collinear Tandem Time-of-Flight Mass Spectrometer for Infrared Photodissociation Spectroscopy of Mass-Selected Ions. *Sci. China: Chem.* **2014**, *57*, 172−177.
(47) Becke, A. D. Density-Functional Thermochemistry. III. The Role of Exact Exchange. *J. Chem. Phys.* **1993**, *98*, 5648−5652.
(48) Krishnan, R.; Binkley, J. S.; Seeger, R.; Pople, J. A. Self-Consistent Molecular-Orbital Methods. 20. Basis Set for Correlated Wave-Functions. *J. Chem. Phys.* **1980**, *72*, 650−654.
(49) Lee, C.; Yang, W.; Parr, R. G. Development of the Colle-Salvetti Correlation-Energy Formula into a Functional of the Electron Density. *Phys. Rev. B* **1988**, *37*, 785−789.
(50) McLean, A. D.; Chandler, G. S. Contracted Gaussian-Basis Sets for Molecular Calculations.1. 2nd Row Atoms, Z = 11−18. *J. Chem. Phys.* **1980**, *72*, 5639−5648.
(51) Frisch, M. J.; Trucks, G. W.; Schlegel, H. B.; Scuseria, G. E.; Robb, M. A.; Cheeseman, G.; Scalmani, J. R.; Barone, V.; Mennucci, B.; Petersson, G. A.; et al. *Gaussian 09*, Revision D.01; Gaussian, Inc.: Wallingford CT, 2013.
(52) Michalak, A.; Mitoraj, M.; Ziegler, T. Bond Orbitals from Chemical Valence Theory. *J. Phys. Chem. A* **2008**, *112*, 1933−1939.
(53) Mitoraj, M. P.; Michalak, A.; Ziegler, T. A Combined Charge and Energy Decomposition Scheme for Bond Analysis. *J. Chem. Theory Comput.* **2009**, *5*, 962−975.
(54) te Velde, G.; Bickelhaupt, F. M.; Baerends, E. J.; Guerra, C. F.; Van Gisbergen, S. J. A.; Snijders, J. G.; Ziegler, T. Chemistry with ADF. *J. Comput. Chem.* **2001**, *22*, 931−967.
(55) Ricks, A. M.; Reed, Z. E.; Duncan, M. A. Infrared Spectroscopy of Mass-Selected Metal Carbonyl Cations. *J. Mol. Spectrosc.* **2011**, *266*, 63−74.
(56) Wang, G.; Chi, C.; Cui, J.; Xing, X.; Zhou, M. Infrared Photodissociation Spectroscopy of Mononuclear Iron Carbonyl Anions. *J. Phys. Chem. A* **2012**, *116*, 2484−2489.
(57) Wang, G. J.; Zhou, M. F. Infrared Spectra, Structures and Bonding of Binuclear Transition Metal Carbonyl Cluster Ions. *Chin. J. Chem. Phys.* **2018**, *31*, 1−11.
(58) Pyykko, P.; Atsumi, M. Molecular Single-Bond Covalent Radii for Elements 1−118. *Chem.—Eur. J.* **2009**, *15*, 186−197.
(59) Saha, R.; Pan, S.; Merino, G.; Chattaraj, P. K. Unprecedented Bonding Situation in Viable $E_2(NHB^{Me})_2$ (E = Be, Mg; NHB^{Me} = $(HCN^{Me})_2B$) Complexes: Neutral E_2 Forms a Single E-E Covalent Bond. *Angew. Chem., Int. Ed.* **2019**, *58*, 8372−8377.
(60) Zhao, L.; von Hopffgarten, M.; Andrada, D. M.; Frenking, G. Energy Decomposition Analysis. *Wiley Interdiscip. Rev. Comput. Mol. Sci.* **2018**, *8*, No. e1345.

https://doi.org/10.1021/acs.jpca.3c02295
J. Phys. Chem. A 2023, 127, 4483−4491